Carbohydrate Polymers, Original full-length research papers

Wood-mimetic skins prepared using horseradish peroxidase catalysis to induce surface wrinkling of chitosan film upon drying

Hironori Izawa[a,*], Yuki Dote[b], Noriko Okuda[a], Masato Sumita[c], Shinsuke Ifuku[a], Minoru Morimoto[d], Hiroyuki Saimoto [a,*]

[a] Graduate School of Engineering, Tottori University, 4-101 Koyama-Minami, Tottori 680-8550, Japan

[b] Faculty of Engineering, Tottori University, 4-101 Koyama-Minami, Tottori 680-8550, Japan

[c] Department of Chemistry, Graduate School of Pure and Applied Sciences, University of Tsukuba, 1-1-1 Tennoudai, Tsukuba, Ibaraki 305-8571, Japan

[d] Division of Instrumental Analysis, Research Center for Bioscience and Technology, Tottori University, Tottori 680-8550, Japan

*Correspondence to: Hironori Izawa and Hiroyuki Saimoto.

Postal Address: Department of Science and Biotechnology, Graduate School of Engineering, Tottori University, 4-101 Koyama-Minami, Tottori 680-8550, Japan.

HI: Phone: +81-857-31-5813. Fax: +81-857-31-5813. E-mail: h-izawa@chem.tottori-u.ac.jp

HS: Phone: +81-857-31-5693. Fax: +81-857-31-5813. E-mail: saimoto@chem.tottori-u.ac.jp

Abstract

We previously developed bio-based wrinkled surfaces induced by wood-mimetic skins upon drying in which microscopic wrinkles were fabricated on a chitosan (CS) film by immersing it in a phenolic acid solution, followed by horseradish peroxidase (HRP)-catalyzed surface reaction and drying. However, the detailed structure of the resulting wood-mimetic skins, including crosslinking mode and thickness, has not been clarified due to the difficulty of the analysis. Here, we prepare wrinkled films using ferulic acid (FE), vanillic acid (VA), and homovanillic acid (HO) and characterize their structures to clarify the unknown characteristics of wood-mimetic skin. Chemical and structural analyses of wood-mimetic skins prepared using VA and HO indicate that the crosslinking structure in the skin is composed of ionic bonds between CS and an oligophenolic residue generated by the HRP-catalyzed reaction on the CS surface. Moreover, the quantity of these ionic bonds is related to the skin hardness and wrinkle size. Finally, SEM and TOF-SIMS analyses indicate that the skin thickness is on the submicron order (<200 nm).

Key Words: Chitosan, Surface wrinkling, Skin layer, Horseradish peroxidase, Phenolic acid, Biomimetic materials

1. Introduction

Biomimetic systems that imitate the design principles of nature are key technologies in the progress toward environmentally benign and high-performance materials (Bhushan, 2009; Bhushan & Jung, 2011). Many functional materials inspired by nature have been developed (Aizenberg & Fratzl, 2013; Kawamura, Kohri, Morimoto, Nannichi, Taniguchi & Kishikawa, 2016; Kawamura, Kohri, Yoshioka, Taniguchi & Kishikawa, 2017; Otsuka, Fujikawa, Yamane & Kobayashi, 2017; Pandian & Sugiyama, 2016; Sedo, Saiz-Poseu, Busque & Ruiz-Molina, 2013).

Surface-wrinkling is a ubiquitous physical process that creates macro/microscopic wrinkles in nature (Genzer & Groenewold, 2006; Ionov, 2012). This spontaneous process is the result of inhomogeneous changes triggered by internal stresses and swelling/shrinking of tissue layers possessing different elastic moduli (Ionov, 2012). The formation of fine wrinkles in human skin is closely associated with decreases in the water content of the stratum corneum by aging; i.e., fine wrinkles are formed by drying, and as a result of inhomogeneous shrinkage (Barel, Paye & Maibach, 2009; Imokawa & Takema, 1993; Tsukahara, Hotta, Fujimura, Haketa & Kitahara, 2007).

Nano/microscopic wrinkled surfaces inspired by nature-mimetic surface designs have been developed for optical (Ohzono, Suzuki, Yamaguchi & Fukuda, 2013) and electronic devices (Lee et al., 2013), the realization of tunable wettability (Li, Dai, John & Carter, 2013) and adhesion (Davis, Martina, Creton, Lindner & Crosby, 2012), and the synthesis of cell culture scaffolds (Zhao, Gu, Zhao, Guan, Zhu & Zhang, 2014). Basically, a skin layer is fabricated on a soft substrate via dry processing methods, including chemical vapor deposition (Bowden, Brittain, Evans, Hutchinson & Whitesides, 1998), photo-crosslinking (Chen, Reed & Yang, 2013), and UV/O_3 oxidation (Efimenko, Rackaitis, Manias, Vaziri, Mahadevan & Genzer, 2005). The wrinkling event can be caused/controlled by mechanical stress (Efimenko, Rackaitis, Manias, Vaziri, Mahadevan & Genzer, 2005), thermal expansion (Bowden, Brittain, Evans, Hutchinson & Whitesides, 1998), and/or swelling-shrinking (Huraux, Narita, Bresson, Fretigny & Lequeux, 2012; Rizzieri, Mahadevan, Vaziri & Donald, 2006; Zhao, Gu, Zhao, Guan, Zhu & Zhang, 2014).

We previously developed a surface-wrinkling system inspired by the fine wrinkles and design principles of wood-cell walls (Fig. 1) (Izawa, Okuda, Ifuku, Morimoto, Saimoto & Rojas, 2015; Izawa et al., 2016). In this method, wood-mimetic skins are fabricated by immersing chitosan (CS) film in a phenolic acid (PH)-methanol solution, then treated with horseradish peroxidase (HRP) to catalyze a surface reaction. Finally, surface wrinkling is

induced by water evaporation during drying. The wrinkle wavelength and amplitude can be controlled by the choice of a phenolic acid (ferulic acid, FE; *p*-coumaric acid, CO; or caffeic acid, CA) and by varying the temperature of the immersion process. Using this system, we found that the wrinkle size was predominately determined by the hardness of the wood-mimetic skins (Izawa et al., 2016). However, the structure of the wood-mimetic skin layer has not been fully elucidated.

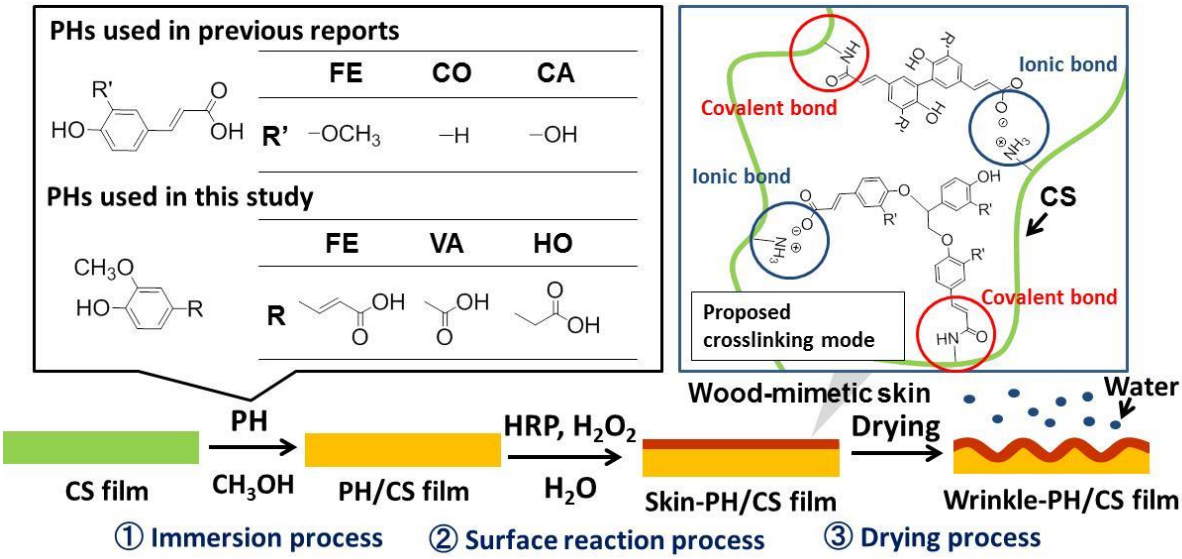

Fig. 1. Illustration of the wood-inspired surface wrinkling systems used in this study and in previous reports.

Using this surface-wrinkling system, a dehydration-condensation reaction was observed between CS and the PHs during the immersion process (Izawa, Okuda, Ifuku, Morimoto, Saimoto & Rojas, 2015). Therefore, we hypothesized that the covalently bound PHs on the CS film acted as reaction sites for chemical and/or ionic crosslinking via the HRP-catalyzed oligomerization of the precursor molecules to yield a skin layer. However, the role of covalently bound PH in skin layer formation has not yet been proved due to the difficulty of analyzing insoluble skin layers. In addition, the detailed crosslinking mode between CS and phenolic oligomers has not been fully clarified.

In common wrinkled surfaces, the wavelength (λ) of the wrinkle is dependent on skin thickness (d), and the mechanical properties of the film are described as follows (Chung, Nolte & Stafford, 2011; Genzer & Groenewold, 2006):

$$\lambda = 2\pi d \left(\frac{\bar{E}_s}{3\bar{E}_f}\right)^{\frac{1}{3}}, \quad (1)$$

where the subscripts *s* and *f* refer to the skin layer and the foundation (substrate), respectively; $\bar{E}$ is the plane-strain modulus given by $E/(1-\nu^2)$, where E is the elastic modulus, and ν is the Poisson's ratio. Thus, the skin thickness is important information for understanding surface wrinkling. However, the skin thickness has not been fully investigated because it is not distinguishable due to its very small thickness, and also because of the similar electron density.

Here, we investigate the unknown characteristics of wood-mimetic skin. To clarify the detailed structure of the skin layers, we use surface wrinkling induced by ferulic acid (FE), vanillic acid (VA), and homovanillic acid (HO), which are PHs having different substituents (R), although always including a carboxyl group (Fig. 1). The previously used HRP-catalyzed reaction of FE generates a phenoxide radical that can resonate with the 5'-position or the β-position (Fig. 2A) (Oudgenoeg et al., 2002). The coupling reaction of these radicals provides oligomers (Izawa, Miyazaki, Ifuku, Morimoto & Saimoto, 2016). However, the HRP-catalyzed reactions of VA and HO provide only dimers (Fig. 2B) (Ci & Wang, 1991; Foppoli, Coccia, Blarzino & Rosei, 2000; Tai, Sawano & Ito, 2012). In addition, the carboxyl groups in FE and VA are conjugated to styryl and phenyl groups, respectively, while that in HO is not conjugated. These differences in the HRP-catalyzed reactions and reactivity of the carboxyl groups provide important information regarding wood-mimetic skin. In addition, we conducted scanning electron microscopic (SEM) and Time-of-Flight secondary ion mass spectrometry (TOF-SIMS) analysis of the wrinkled surface to estimate the skin thickness and structure.

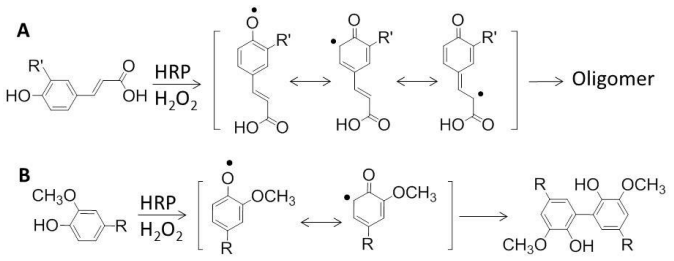

Fig. 2. Previously reported HRP-catalyzed reactions of FE (A) and VA or HO (B).

2. Experiments

2.1. Materials

CS (M_n: 5.6 x 10^4; M_w/M_n: 2.36; GPC analysis with Pullulan standards) was supplied by the Koyo Chemical Co., Ltd. (Tottori, Japan), with an undeacetylated 23.5% fraction of CS (elemental analysis). FE, HO, and VA were purchased from the Tokyo Chemical Industry Co., Ltd. (Tokyo, Japan). HRP (274 U/mg) was purchased from Toyobo Co., Ltd. (Osaka, Japan). Other reagents were commercial grade and used without further purification.

2.2. Instrumentation

SEM images of film surfaces were recorded by a TM303Plus (Hitachi, Japan) without coating. SEM cross-sectional images were recorded with a JSM-6700F (JEOL, Japan). The sample was coated with an approximately 5 nm layer of Pt with an ion sputter coater. The wrinkle amplitudes of the wrinkled films were obtained with a NanoCute-NanoNavi IIs (Seiko Instruments, Japan). Elemental analysis data were recorded on a Perkin Elmer 2400 II CHNS/O (Perkin Elmer, US). Infrared (IR) spectra of the samples were recorded by a Spectrum 65 (Perkin-Elmer Japan Co., Ltd., Japan) equipped with an ATR attachment. TOF-SIMS measurement was performed with a PHI TRIFT V nanoTOF (ULVAC-PHI, Japan). The pulsed primary ion source was Bi_3^{2+}, and the ion beam was operated at 30 kV (50 fA AC) with a 50 μm x 50 μm rastering area at an incident angle of 45°. The sputtering was done with

an Ar^+ ion beam operated at 300 V and 150 nA with a 0.1 mm x 0.1 mm rastering area at an incident angle of 45°.

2.3. Preparation of the CS film

CS (2.0 g) was dissolved in 100 mL of an acidic aqueous solution containing 0.5 mL acetic acid. Then, 10 mL of the CS solution was added to a Teflon Petri dish (φ=50 mm) and degassed under reduced pressure. The CS solution was heated at 50˚C for 24 h to yield a CS film after evaporation. The film was then heated at 50˚C under reduced pressure for 12 h. The inhomogeneous edge of the film was cut down with scissors. The weight and thickness of the CS film were ca 0.15 g and 111±12 μm, respectively.

2.4. Surface wrinkling of films

In a typical experiment, a CS film was immersed in 20 mL methanol containing 0.05 g/mL FE at 30˚C for 24 h. The resulting film (hereafter, FE/CS film) was removed and soaked in 10 mL water, followed by the prompt addition of the HRP (1 mL, 137 U) and H_2O_2 (200 μL, 30% concentration). The system was kept at 30˚C for 12 h, after which the film was removed and dried at 40˚C under for 12 h.

3. Results and Discussion

3.1 Morphology of the obtained films

Figures 3A-F show plane-view SEM images of the surface of the wrinkled films. A detailed characterization of the wrinkles formed is provided in Fig. 3G. In the case of FE, the results were almost the same as that in our previous report (Izawa, Okuda, Ifuku, Morimoto, Saimoto & Rojas, 2015), in which the mean wrinkle wavelengths and amplitudes under immersion treatments at 30˚C and 40˚C were 1.42±0.34 and 0.97±0.22 μm, respectively, and 0.52±0.15 and 0.39±0.10 μm, respectively. The mean wrinkle wavelengths and amplitudes at

40˚C immersion were smaller than those at 30˚C. In this wrinkling system, higher temperatures on the immersion process led to the formation of softer skins, due to the harder decomposition of the CS around the film surface, inducing smaller wrinkles (Izawa et al., 2016). Note that wrinkled surfaces were not observed on the FE/CS films, the control CS film prepared by the adsorption of oligomeric FE, and the original CS film (Figures S1A-B, S1C, and S1D, respectively). For VA, surprisingly, wrinkling occurred during both the 30˚C and 40˚C immersion treatments, even though the HRP-catalyzed reaction of VA only provided the dimer as described above. The mean wrinkle wavelengths and amplitudes at 30˚C and 40˚C were 3.07±0.17 and 1.61±0.25 μm, respectively, and 0.62±0.24 and 0.30±0.10 μm, respectively, which were larger than those of the FE/CS system. This result suggests that VA produces harder skin, even though the HRP-catalyzed reaction of VA provides just the dimer. When HO was used, wrinkling was observed on the wrinkle-HO/CS film at an immersion temperature of 40˚C. The mean wrinkle wavelength and amplitude under treatments at 40˚C were 2.96±0.16 μm and 0.68±0.18 μm, respectively, which were larger than those for the VA/CS system at 40˚C. No wrinkling occurred at 30˚C. The same phenomenon was observed in the CA/CS system. There was the suggestion that no wrinkling is due to a lack of crosslinking reaction sites on the CA/CS film (Izawa, Okuda, Ifuku, Morimoto, Saimoto & Rojas, 2015). The results obtained with VA and HO clearly indicated that the vinyl moiety in FE is not needed to induce surface wrinkling. Note that we additionally confirmed the absence of wrinkling by using 2-methoxyphenol, without a carboxyl group, for the treatment at 30˚C and 40˚C.

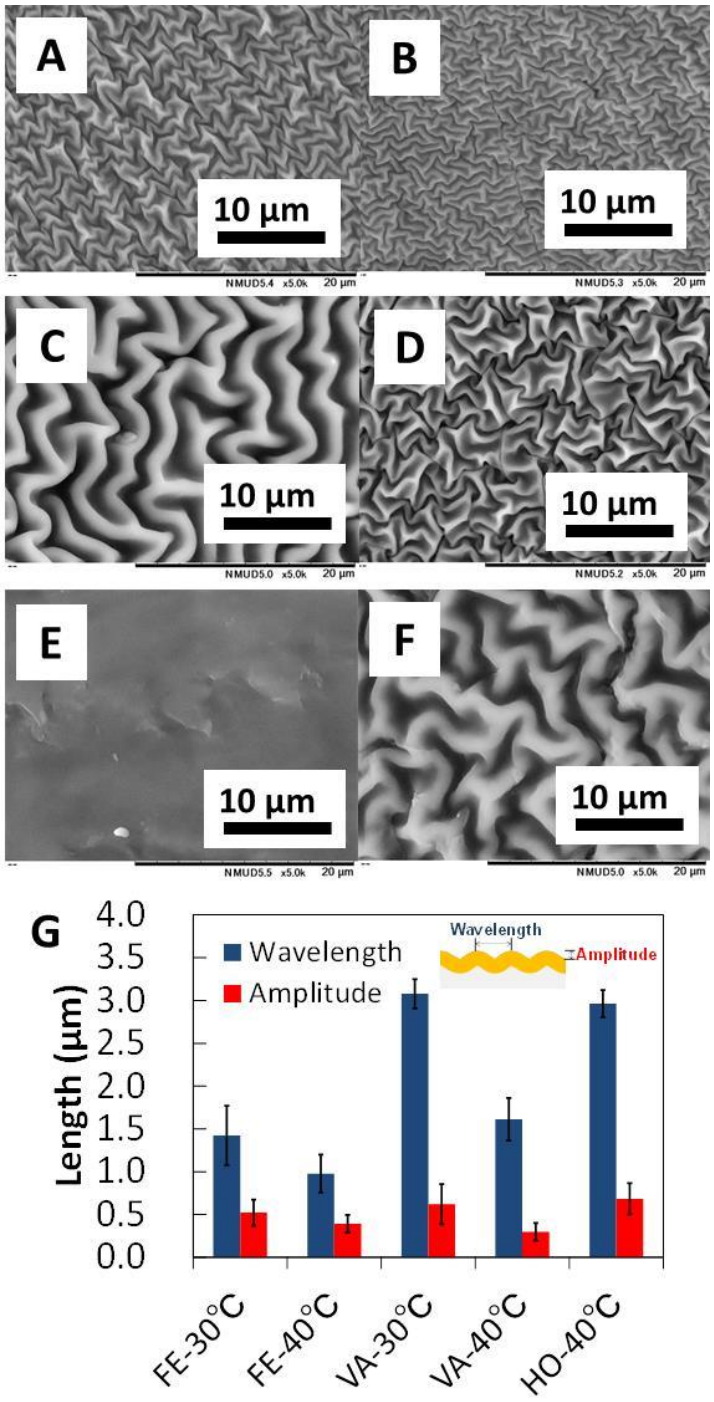

Fig. 3. Plane-view SEM images of the films obtained via immersion treatment at 30˚C (A) or 40˚C (B) using FE, via immersion treatment at 30˚C (C) or 40˚C (D) using VA, and via immersion treatment at 30˚C (E) or 40˚C (F) using HO and their mean wavelength and amplitude of wrinkles (G).

3.2 Characterization of the film surfaces

To confirm the presence of covalently bound PHs on the CS film, the PH/CS films were Soxhlet-extracted with methanol for 1 week in order to remove any unreacted PH, and the IR spectra of the film surfaces were measured (Fig. 4A). In the 30˚C treatment, the absorption peaks attributed to aromatic -C=C- (Swislocka, Kowczyk-Sadowy, Kalinowska & Lewandowski, 2012) appeared at around 1540 cm^{-1} for the FE/CS and VA/CS systems. The absorption peaks observed even after Soxhlet-extraction indicated the presence of the covalently bound PH via an amide bond on the CS film. In contrast, this was not seen in the HO/CS system at this temperature. We considered that the lack of a peak observed on the HO/CS system was due to the lower reactivity of unconjugated carboxyl groups than in FE and VA. On the other hand, the absorption peak due to aromatic -C=C- was observed in the HO/CS system in the 40˚C treatment. These observations are consistent with the wrinkling results. Thus, this result confirmed our previous speculation that the carboxyl group in PH plays a critical role in the formation of covalently bound PH, acting as a reaction site for the HRP-catalyzed reaction to form the skin layer (Fig. 4B).

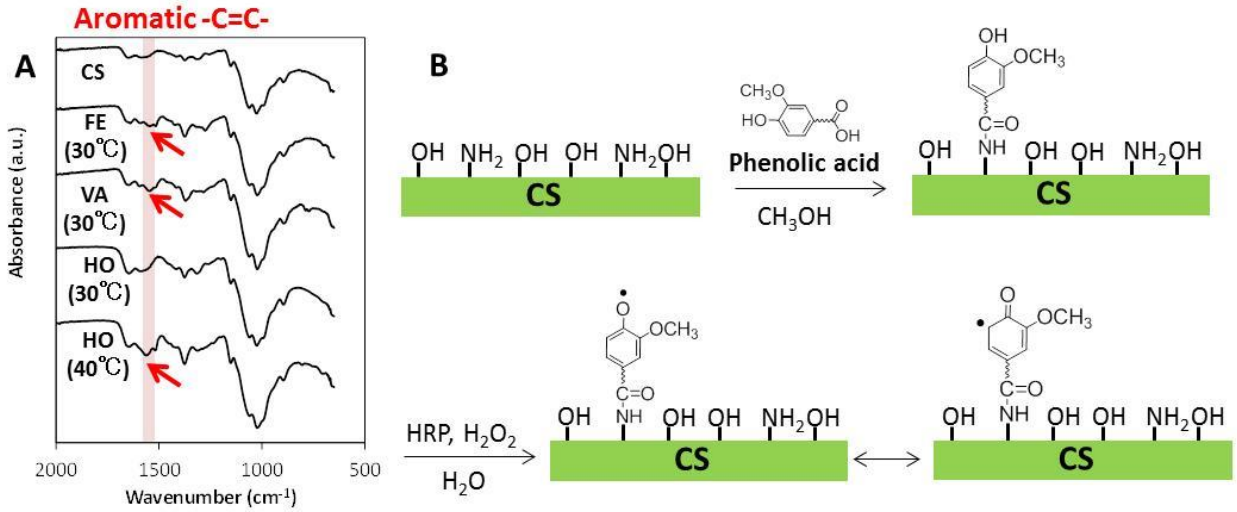

Fig. 4. IR spectra of the extracted FE/CS, VA/CS, HO/CS films and CS (A), and illustration of the confirmed role of covalently bound PH (B).

In order to analyze the chemical structure of the skin, we performed IR analysis of the wrinkle-FE/CS, VA/CS, and HO/CS films from the 40˚C treatment (Fig. 5). In the wrinkle-FE/CS film spectrum, the absorption peaks attributed to $-COO^-$ and $-NH_3^+$ (Hu, Jiang, Ding, Ge, Yuan & Yang, 2002) were observed at 1565 cm^{-1} and 1630 cm^{-1}, respectively. Meanwhile, absorption peaks due to aromatic alkene and glycosidic ether were observed as significant ones at 1511 cm^{-1} and 1024 cm^{-1}, respectively, indicating the skin layer was composed of both CS and oligomeric FE. By using VA, the absorption peak due to $-COO^-$ was slightly enhanced compared to that of the wrinkle-FE/CS film. Interestingly, using HO further enhanced the absorption peak attributed to $-COO^-$, to the point where the absorption peak attributed to the aromatic alkene was completely overlapped by it. These results suggested a higher quantity of the ionic bonds in the case of VA and HO than in FE. Indeed, the HRP-catalyzed reaction of FE involves decarboxylation that reduces the quantity of the carboxyl group in the system (Oudgenoeg et al., 2002). In addition, it was suggested that there was a higher quantity of the ionic bonds in the HO/CS system than in the VA/CS system. As described above, the products from the HRP-catalyzed reaction of VA and HO are dimers with a biphenyl framework (Fig. 2B). The only structural difference between those dimers is whether the methylene spacer is present or not. The carboxyl group in HO has higher mobility than that of the VA by virtue of the methylene spacer. We consider that the higher mobility facilitates ionic bonding in the HO/CS system.

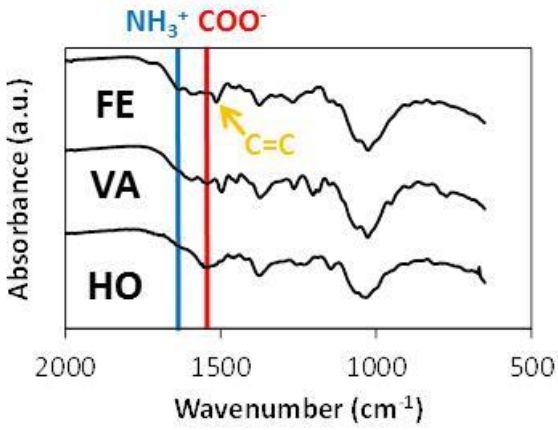

Fig. 5. IR spectra of surfaces of the wrinkle-FE/CS, VA/CS, and HO/CS films.

There are three possible crosslinking modes in the VA/CS and HO/CS systems. The first is the covalently crosslinked structure generated by the radical coupling of each of the covalently bound PHs (Fig. 6A). The second is the ionically crosslinked structure between a dimeric side chain, generated by radical coupling of PH and the covalently bound PH, and CS (Fig. 6B). The third and final possible modes are the ionically crosslinked structure composed of CS and dimeric PH (Fig. 6C). When covalently bound HO was not formed, surface wrinkling did not occur, as mentioned above. Therefore, this third crosslinking mode is not important for skin layer formation. Indeed, the top layers fabricated by the adsorption of oligomers on the CS film could not induce surface wrinkling (Fig. S1C). Elemental analysis of the VA/CS and HO/CS films and the extracted VA/CS and HO/CS films provided evidence that the VA/CS and HO/CS films included ca 50-fold greater amounts of VA and HO than covalently bound VA and HO, respectively. Under this condition, the radical coupling of PH and the covalently bound PH proceeds more readily than that between the covalently bound PHs themselves. In addition, the HRP-catalyzed reaction of the extracted VA/CS and HO/CS films did not provide wrinkled surfaces upon drying. Thus, the second crosslinking mode is the most likely crosslinking structure for the VA/CS and HO/CS systems. This is important information which suggests that ionic crosslinking by the dimeric/oligomeric side chain is capable of surface wrinkling upon drying. In addition, we observed a crucial phenomenon that underscored the importance of the ionic bonding for the skin formation. Namely, the wrinkles were maintained in water even after 1 week, while they disappeared in 100 mM NaOH aqueous solution due to the dissociation of the ionic bond (Fig. S2), indicating that the wood-mimetic skins were formed by ionic crosslinking.

Our theoretical calculations (see Table S1) show that the ionic bonds between glucosamine and each of the PHs (FE, VA, HO) have the similar strength. Thus, the

production of larger wrinkles in the VA/CS and HO/CS systems could be explained by the quantity of the ionic bonds. The order of the speculated quantity of the ionic bonds by IR analysis was as follows: the HO/CS system > VA/CS system > FE/CS system. The wrinkle wavelengths and amplitudes decreased in the following order: the HO/CS system > the VA/CS > the FE/CS. This relation indicates that a higher quantity of the ionic bonds results in a harder skin layer, leading to larger wrinkling (Izawa et al., 2016).

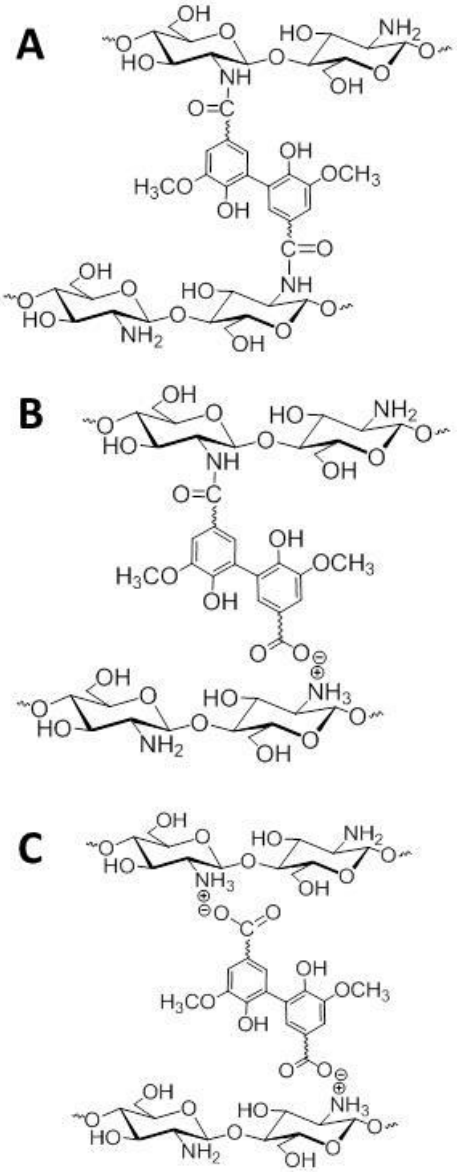

Fig. 6. Possible crosslinking structure in the VA/CS and HO/CS systems.

3.3 SEM and TOF-SIMS analysis for the skin layer

Figure 7 shows an SEM image of the cross-section of the wrinkle-FE/CS film. The topmost layer, which is considered to be the skin layer, is shown. This topmost layer was approximately 120 nm thickness. Fig. 8A shows TOF-SIMS spectra of positively charged secondary ions produced from the wrinkled surface. Characteristic fragment ions for the α,β-unsaturated carboxylic acid groups of oligomeric FE moieties in the skin layer were observed at *m/z* 41 ($C_3H_5^+$), 55 ($C_3H_3O^+$), and 69 ($C_4H_5O^+$) (Lawrence, Tripathi & Jeyakumar, 2009; Pati, Crupi, Benucci, Antonacci, Di Luccia & Esti, 2014). The depth profiles of the characteristic fragment ions are illustrated in Fig. 8B. The intensities of these peaks were linearly decreased with the increase in the sputter time. The negative slope increased after 420 s. The depth profile for impurities (Na^+ and K^+) were completely different from those for the characteristic peaks, which were exponential decay curves. These results imply that the component of the topmost layer changes after 420 s. The depth at 420 s under the sputter condition for SiO_2 was ca 40 nm. The sputter rate for the organic materials was 2-4 times higher than for the SiO_2 (Fearn, 2015). This observation shows good agreement with the observed thickness of the topmost layer. Thus, this result indicates the topmost layer observed in the SEM analysis is the wood-mimetic skin, and the thickness of the skin layer is on the submicron order (<200 nm). Note that the thickness of wood-mimetic skins produced by the HRP-catalyzed reaction does not depend on the choice of PH or the conditions of the immersion process, because the previously reported correlation between the wrinkle sizes and mechanical properties indicated that there was no large difference in the skin thicknesses of the wrinkled films prepared under different immersion conditions (Izawa et al., 2016).

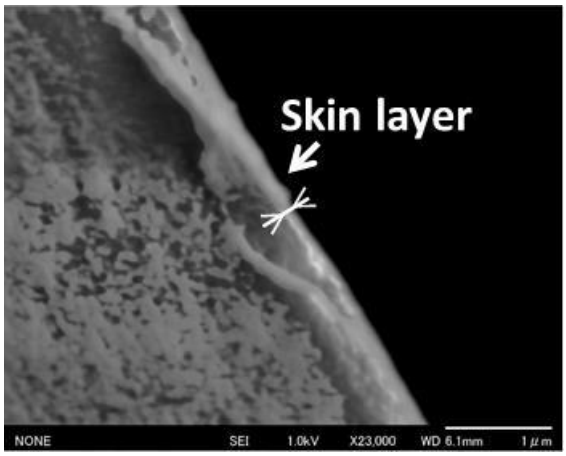

288

289 **Fig. 7.** SEM cross-section image of the wrinkle-FE/CS film. Scale bar is 1 μm.

290

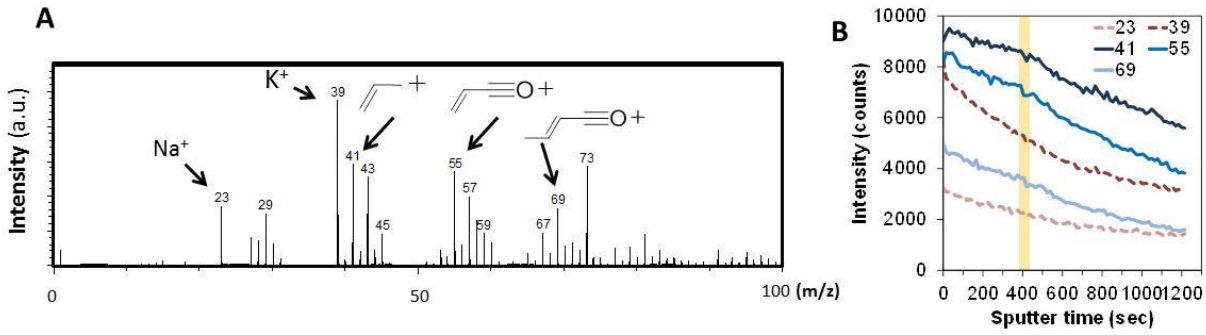

291

292 **Fig. 8.** TOF-SIMS spectrum (A) of the wrinkle-FE/CS film and depth profile of the
293 characteristic fragment ions (B).

294

295 ## 4. Conclusion

296 We have analyzed the chemical and structural characteristics of wood-mimetic skins that
297 were produced by a horseradish peroxidase (HRP)-catalyzed reaction of ferulic acid (FE),
298 vanillic acid (VA), and homovanillic acid (HO) on a chitosan (CS) film and that exhibited
299 surface wrinkling upon drying. When HO was used, covalently bound HO was not observed
300 on immersion treatment at 30˚C. This means that no wrinkling occurred at this temperature. In
301 contrast, wrinkled surfaces were observed when covalently bound FE, VA, and HO were
302 formed. Therefore, we determined that the carboxyl group in PH plays a critical role in that
303 the formation of covalently bound PH acts as a reaction site for the HRP-catalyzed reaction to

form the skin layer. In addition, the observation of surface wrinkling using VA and HO revealed that an ionic crosslinking structure composed of CS and dimeric phenolic acid residues on CS enables skin layer formation, and induces surface wrinkling upon drying. Furthermore, SEM and TOF-SIMS analyses indicated that the thickness of the skin layer was on the order of submicrons (<200 nm). This study underscores the importance of ionic crosslinking for skin layer formation. This perspective should result in novel polysaccharide-based wrinkled materials being created for application to various fields.

Acknowledgements

This work was supported in part by JSPS KAKENHI Grant Number 16K05916. Partial support was also provided by the NIMS Microstructural Characterization Platform, which is a program of the Nanotechnology Platform of the Ministry of Education, Culture, Sports, Science and Technology (MEXT), Japan.

References

Aizenberg, J., & Fratzl, P. (2013). New Materials through Bioinspiration and Nanoscience. *Advanced Functional Materials, 23*(36), 4398-4399.

Barel, A. O., Paye, M., & Maibach, H. (2009). *Handbook of Cosmetic Science and Technology*. London: CRC Press.

Bhushan, B. (2009). Biomimetics: lessons from nature - an overview. *Philosophical Transactions of the Royal Society a-Mathematical Physical and Engineering Sciences, 367*(1893), 1445-1486.

Bhushan, B., & Jung, Y. C. (2011). Natural and biomimetic artificial surfaces for superhydrophobicity, self-cleaning, low adhesion, and drag reduction. *Progress in Materials Science, 56*(1), 1-108.

Bowden, N., Brittain, S., Evans, A. G., Hutchinson, J. W., & Whitesides, G. M. (1998). Spontaneous formation of ordered structures in thin films of metals supported on an elastomeric polymer. *Nature, 393*(6681), 146-149.

Chen, C. M., Reed, J. C., & Yang, S. (2013). Guided wrinkling in swollen, pre-patterned photoresist thin films with a crosslinking gradient. *Soft Matter, 9*(46), 11007-11013.

Chung, J. Y., Nolte, A. J., & Stafford, C. M. (2011). Surface Wrinkling: A Versatile Platform for Measuring Thin-Film Properties. *Advanced Materials, 23*(3), 349-368.

Ci, Y. X., & Wang, F. (1991). Catalytic Effects of Peroxidase-Like Metalloporphyrins on the Fluorescence Reaction of Homovanillic-Acid with Hydrogen-Peroxide. *Fresenius Journal of Analytical Chemistry, 339*(1), 46-49.

Davis, C. S., Martina, D., Creton, C., Lindner, A., & Crosby, A. J. (2012). Enhanced Adhesion of Elastic Materials to Small-Scale Wrinkles. *Langmuir, 28*(42), 14899-14908.
Efimenko, K., Rackaitis, M., Manias, E., Vaziri, A., Mahadevan, L., & Genzer, J. (2005). Nested self-similar wrinkling patterns in skins. *Nature Materials, 4*(4), 293-297.
Fearn, S. (2015). *An Introduction to Time-of-Flight Secondary Ion Mass Spectrometry* Bristol: IOP Publishing.
Foppoli, C., Coccia, R., Blarzino, C., & Rosei, M. A. (2000). Formation of homovanillic acid dimer by enzymatic or Fenton system - catalyzed oxidation. *The International Journal of Biochemistry & Cell Biology, 32*(6), 657-663.
Genzer, J., & Groenewold, J. (2006). Soft matter with hard skin: From skin wrinkles to templating and material characterization. *Soft Matter, 2*(4), 310-323.
Hu, Y., Jiang, X. Q., Ding, Y., Ge, H. X., Yuan, Y. Y., & Yang, C. Z. (2002). Synthesis and characterization of chitosan-poly(acrylic acid) nanoparticles. *Biomaterials, 23*(15), 3193-3201.
Huraux, K., Narita, T., Bresson, B., Fretigny, C., & Lequeux, F. (2012). Wrinkling of a nanometric glassy skin/crust induced by drying in poly(vinyl alcohol) gels. *Soft Matter, 8*(31), 8075-8081.
Imokawa, G., & Takema, Y. (1993). Fine wrinkle formation. Etiology and prevention. *Cosmet Toilet, 108*, 65-77.
Ionov, L. (2012). Biomimetic 3D self-assembling biomicroconstructs by spontaneous deformation of thin polymer films. *Journal of Materials Chemistry, 22*(37), 19366-19375.
Izawa, H., Miyazaki, Y., Ifuku, S., Morimoto, M., & Saimoto, H. (2016). Fully Biobased Oligophenolic Nanoparticle Prepared by Horseradish Peroxidase-catalyzed Polymerization. *Chemistry Letters, 45*(6), 631-633.
Izawa, H., Okuda, N., Ifuku, S., Morimoto, M., Saimoto, H., & Rojas, O. J. (2015). Bio-based Wrinkled Surfaces Harnessed from Biological Design Principles of Wood and Peroxidase Activity. *ChemSusChem, 8*(22), 3892-3896.
Izawa, H., Okuda, N., Moriyama, A., Miyazaki, Y., Ifuku, S., Morimoto, M., & Saimoto, H. (2016). Biobased Wrinkled Surfaces Induced by Wood Mimetic Skins upon Drying: Effect of Mechanical Properties on Wrinkle Morphology. *Langmuir, 32*(48), 12799-12804.
Kawamura, A., Kohri, M., Morimoto, G., Nannichi, Y., Taniguchi, T., & Kishikawa, K. (2016). Full-Color Biomimetic Photonic Materials with Iridescent and Non-Iridescent Structural Colors. *Scientific Reports, 6*.
Kawamura, A., Kohri, M., Yoshioka, S., Taniguchi, T., & Kishikawa, K. (2017). Structural Color Tuning: Mixing Melanin-Like Particles with Different Diameters to Create Neutral Colors. *Langmuir, 33*(15), 3824–3830.
Lawrence, R., Tripathi, P., & Jeyakumar, E. (2009). Isolation, Purification and Evaluation of Antibacterial Agents from Aloe Vera. *Brazilian Journal of Microbiology, 40*(4), 906-915.
Lee, S. G., Kim, H., Choi, H. H., Bong, H., Park, Y. D., Lee, W. H., & Cho, K. (2013). Evaporation-Induced Self-Alignment and Transfer of Semiconductor Nanowires by Wrinkled Elastomeric Templates. *Advanced Materials, 25*(15), 2162-2166.
Li, Y. Y., Dai, S. X., John, J., & Carter, K. R. (2013). Superhydrophobic Surfaces from Hierarchically Structured Wrinkled Polymers. *Acs Applied Materials & Interfaces, 5*(21), 11066-11073.
Ohzono, T., Suzuki, K., Yamaguchi, T., & Fukuda, N. (2013). Tunable Optical Diffuser Based on Deformable Wrinkles. *Advanced Optical Materials, 1*(5), 374-380.
Otsuka, T., Fujikawa, S., Yamane, H., & Kobayashi, S. (2017). Green polymer chemistry: the biomimetic oxidative polymerization of cardanol for a synthetic approach to 'artificial urushi'. *Polymer Journal, 49*(3), 335-343.
Oudgenoeg, G., Dirksen, E., Ingemann, S., Hilhorst, R., Gruppen, H., Boeriu, C. G., Sr, P., van Berkel, W. J. H., Laane, C., & Voragen, A. G. J. (2002). Horseradish peroxidase-

catalyzed oligomerization of ferulic acid on a template of a tyrosine-containing tripeptide. *Journal of Biological Chemistry, 277*(24), 21332-21340.
Pandian, G. N., & Sugiyama, H. (2016). Nature-Inspired Design of Smart Biomaterials Using the Chemical Biology of Nucleic Acids. *Bulletin of the Chemical Society of Japan, 89*(8), 843-868.
Pati, S., Crupi, P., Benucci, I., Antonacci, D., Di Luccia, A., & Esti, M. (2014). HPLC-DAD-MS/MS characterization of phenolic compounds in white wine stored without added sulfite. *Food Research International, 66*, 207-215.
Rizzieri, R., Mahadevan, L., Vaziri, A., & Donald, A. (2006). Superficial wrinkles in stretched, drying gelatin films. *Langmuir, 22*(8), 3622-3626.
Sedo, J., Saiz-Poseu, J., Busque, F., & Ruiz-Molina, D. (2013). Catechol-Based Biomimetic Functional Materials. *Advanced Materials, 25*(5), 653-701.
Swislocka, R., Kowczyk-Sadowy, M., Kalinowska, M., & Lewandowski, W. (2012). Spectroscopic (FT-IR, FT-Raman, H-1 and C-13 NMR) and theoretical studies of p-coumaric acid and alkali metal p-coumarates. *Spectroscopy-an International Journal, 27*(1), 35-48.
Tai, A., Sawano, T., & Ito, H. (2012). Antioxidative Properties of Vanillic Acid Esters in Multiple Antioxidant Assays. *Bioscience Biotechnology and Biochemistry, 76*(2), 314-318.
Tsukahara, K., Hotta, M., Fujimura, T., Haketa, K., & Kitahara, T. (2007). Effect of room humidity on the formation of fine wrinkles in the facial skin of Japanese. *Skin Research and Technology, 13*(2), 184-188.
Zhao, Z. Q., Gu, J. J., Zhao, Y. N., Guan, Y., Zhu, X. X., & Zhang, Y. J. (2014). Hydrogel Thin Film with Swelling-Induced Wrinkling Patterns for High-Throughput Generation of Multicellular Spheroids. *Biomacromolecules, 15*(9), 3306-3312.

Figure Captions

Fig. 1. Illustration of the wood-inspired surface wrinkling systems used in this study and in previous reports.

Fig. 2. Previously reported HRP-catalyzed reactions of FE (A) and VA or HO (B).

Fig. 3. Plane-view SEM images of the films obtained via immersion treatment at 30˚C (A) or 40˚C (B) using FE, via immersion treatment at 30˚C (C) or 40˚C (D) using VA, and via immersion treatment at 30˚C (E) or 40˚C (F) using HO and their mean wavelength and amplitude of wrinkles (G).

Fig. 4. IR spectra of the extracted FE/CS, VA/CS, HO/CS films and CS, and illustration of the confirmed role of covalently bound PH (B).

Fig. 5. IR spectra of surfaces of the wrinkle-FE/CS, VA/CS, and HO/CS films.

Fig. 6. Possible crosslinking structure in the VA/CS and HO/CS systems.

Fig. 7. SEM cross-section image of the wrinkle-FE/CS film. Scale bar is 1 μm.

Fig. 8. TOF-SIMS spectrum (A) of the wrinkle-FE/CS film and depth profile of the characteristic fragment ions (B).